Dominant modes of interannual variability in Australian rainfall analyzed using wavelets

Seth Westra[1] and Ashish Sharma[1]

Received 20 March 2005; revised 20 October 2005; accepted 9 November 2005; published 2 March 2006.

[1] One of the key aspects to better managing water resources in Australia is to understand the causes of medium- to long-term rainfall variability, which results in both droughts and periods of above average rainfall and flooding. Much of the research on this variability has focused on the El Niño–Southern Oscillation (ENSO) phenomenon, using methods that assume the relationships between ENSO and Australian rainfall are both linear and stationary. In this paper we present an alternative approach based on wavelets to analyze the dominant modes of variability in three rainfall characteristics: (1) the total annual rainfall, (2) the annual number of wet days, and (3) the maximum annual daily rainfall. We then use a wavelet regression approach to examine the extent of the variability that can be associated with ENSO. The results show that time series of total annual rainfall and annual number of wet days exhibit significant variability at periods of 2.6, 4.6, 7 and 13 years in various locations throughout the country and that these periodicities are not caused directly by the ENSO phenomenon. While maintaining that ENSO still plays a significant role in influencing rainfall variability in Australia, these results highlight the importance of looking beyond ENSO to identify dominant sources of variability in the characteristics of annual Australian rainfall that were studied. In contrast, no coherent modes of variability could be found for the maximum annual daily rainfall time series, highlighting the greater level of random behavior in the intensity of larger rainfall events compared with the long-term averages.

Citation: Westra, S., and A. Sharma (2006), Dominant modes of interannual variability in Australian rainfall analyzed using wavelets, *J. Geophys. Res.*, *111*, D05102, doi:10.1029/2005JD005996.

1. Introduction

[2] One of the significant challenges to water resource managers around the world is to balance an uncertain and variable supply of precipitation with an ever increasing demand for a stable source of fresh water. This is particularly difficult for countries such as Australia, in which the climate is frequently characterized by cycles of severe and sustained drought followed by periods of above average rainfall and widespread flooding. In response, a significant quantity of research has been undertaken with the aim of better understanding and forecasting this variability so that water resource managers can be informed about the potential for water supply shortages or extreme flooding.

[3] Much of the early research on Australian climate variability has focused on the El Niño Southern Oscillation (ENSO) phenomenon [*Quayle*, 1929; *Pittock*, 1975; *Nicholls and Woodcock*, 1981], which has been shown to influence aspects of the climate such as seasonally averaged rainfall, streamflow and drought across much of the Australian continent [*Nicholls et al.*, 1996; *Chiew et al.*, 1998]. Despite the initial optimism of using ENSO to predict Australian rainfall, recent studies have demonstrated that the ENSO phenomenon provides just a part of the picture of what causes the rainfall to be so variable. For instance, it is now known that the impact of ENSO on Australian rainfall varies over time [e.g., *McBride and Nicholls*, 1983; *Cordery and Opoku-Ankomah*, 1994], and may be modulated by the lower-frequency Interdecadal Pacific Oscillation [*Mantua et al.*, 1997; *Zhang et al.*, 1997; *Power et al.*, 1998, 1999a, 1999b; *Verdon et al.*, 2004]. The impact of long-term variability in the Indian Ocean is also known to be important, particularly in the western parts of the continent [*Nicholls*, 1989; *Drosdowsky*, 1993], and it is hypothesized that Indian Ocean sea surface temperatures (SSTs) may have a modulating influence on the ENSO-rainfall relationship over the southeast of the country [*Drosdowsky*, 2002].

[4] The results of these and other studies suggest that any method that aims to characterize the long-term variability of rainfall in Australia must take into account the highly nonstationary relationship between climatic phenomena such as ENSO, and Australian rainfall [e.g., *Cordery and Opoku-Ankomah*, 1994]. Nevertheless, some of the commonly used methods of analyzing Australian rainfall such as correlation analysis or Fourier methods have only limited ability at interpreting relationships that change over time. In contrast, this study uses a method based on wavelets theory to analyze long-term records of Australian point rainfall, so that the nonstationary and nonlinear characteristics of cli-

[1]School of Civil and Environmental Engineering, University of New South Wales, Sydney, New South Wales, Australia.

0148-0227/06/2005JD005996$09.00

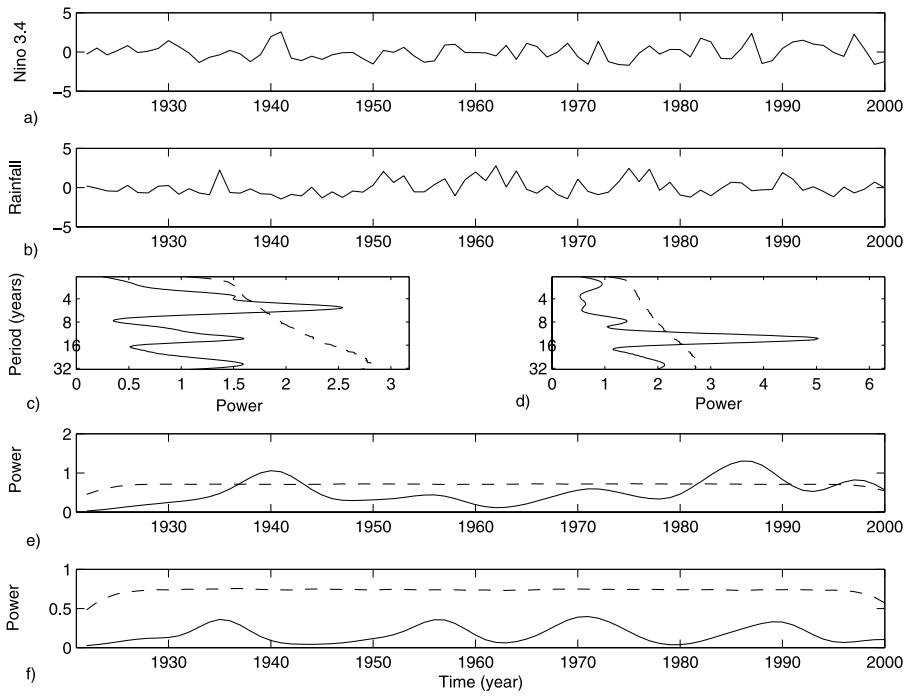

Figure 1. Normalized time series of (a) the Niño 3.4 SST data set and (b) total annual rainfall from a gauging station located in Jervis Bay, along the east coast of Australia. (c and d) Global wavelet spectra for these series, which represent the wavelet power averaged in time. (e and f) Scale-averaged wavelet spectra, which represent the wavelet power in the 3 to 6 year band. Confidence intervals for Figures 1c–1f are represented as dashed lines and are at the 95% significance level.

matic time series may be analyzed. Wavelets are used in this analysis as they are able break the time series into both the time and frequency domains. Thus the approach is related to windowed Fourier transforms, except that whereas windowed Fourier transforms use a constant window size to analyze both high- and low-frequency components, the wavelet analysis is scale-independent, and is therefore better suited to analyses where a wide range of frequencies may be present. The wavelets approach is therefore a much more efficient method of capturing not only the dominant frequency modes of a given time series, but also the manner in which these frequency modes change over time [*Torrence and Compo*, 1998].

[5] To illustrate this, we examine the relationship between the Niño 3.4 time series, an indicator of the ENSO phenomenon, and a total annual rainfall time series from a gauging station located along the east coast of Australia, as shown in Figures 1a and 1b, respectively. Traditional correlation analysis reveals that these time series are correlated concurrently at the 95% significance level, which agrees with earlier studies that show a strong relationship between rainfall and ENSO along much of eastern Australia [*Cai et al.*, 2001]. Now consider the global wavelet spectra for both time series in Figures 1c and 1d. These plots show the wavelet power averaged over the entire time series for frequencies ranging from 2 to 32 years, and are able to show how two time series compare with each other in the frequency domain. The 95% significance levels for the wavelet analysis are represented as dashed lines, and have been derived using a Monte Carlo approach described in more detail in section 2.2 below. Examining the Niño 3.4 time series first, it can be seen that there is significant variability with a period of about 5 years, which is within the 3 to 6 year frequency band that is traditionally associated with ENSO variability [*Trenberth*, 1997]. In contrast, the global wavelet spectrum of the total annual rainfall time series shows the presence of significant variability with a period of 13 years, and therefore cannot be directly related to the ENSO phenomenon, but may be linked to an interdecadal phenomenon such as the Interdecadal Pacific Oscillation (IPO) [*Power et al.*, 1999a].

[6] Finally, the scale-averaged wavelet spectra for both time series are provided in Figures 1e and 1f, and show the wavelet power averaged over the 3 to 6 year band. If the relationship between ENSO and the total annual rainfall time series is as strong as is suggested by the correlation analysis, then the timing associated with the maximum ENSO variability in the 3 to 6 year band should be reflected in the rainfall time series. This is not the case, however, with the variability associated with the rainfall time series in this band shown to be statistically insignificant for the full duration analyzed.

[7] These results and others presented later in this paper raise a number of interesting questions regarding the links between ENSO and Australian rainfall. For example, what does a statistically significant correlation suggest about the strength of the link between the ENSO time series and Australian rainfall? Similarly, what does variability in the 3 to 6 year band suggest about the presence or absence of a relationship between a particular rainfall time series and ENSO? Are there distinct regions in Australia whose rainfall time series exhibit significant variability at specific

frequency levels? Does one note the same type of variability in annual rainfall as in the maximum daily rainfall? Finally, is it possible to identify other long-term climatic trends in Australian rainfall that are not directly associated with ENSO? This study will show how wavelet theory can assist in answering these questions, so that the contributing factors to rainfall variability in Australia can be better understood.

[8] The rest of this paper is organized as follows. A description of the wavelet analysis method is provided in section 2. The rainfall and climate (ENSO) data used in this study are outlined in section 3. In section 4, we present the results of the wavelet analysis, with a focus on identifying regions of coherent variability and examining the degree to which this variability is influenced by ENSO. The conclusions from this study are presented in section 5.

2. Wavelets Methodology

2.1. An Introduction to Wavelets

[9] Wavelets are becoming an increasingly popular mathematical tool for the analysis of time series that have nonstationary power at a range of frequencies [*Torrence and Compo*, 1998], and the technique has already been successfully applied in the analysis of a wide range of climatic time series [e.g., *Gu and Philander*, 1995; *Lau and Weng*, 1995; *Torrence and Webster*, 1998; *Jain and Lall*, 2001]. Their popularity stems from their ability to provide localized information on a time series in both the time and the frequency domains, by representing the series using scaled and translated versions of a wavelet basis function. A wide variety of such wavelet functions are available, which can be tailored to the specific time series to be analyzed. This contrasts with the more traditional Fourier methods, which are based on a single sinusoidal function. A further difference between wavelet and Fourier methods is that the time and frequency localization of the wavelet transform allows the efficient representation of a time series with changing frequencies, as illustrated through a synthetic example presented by *Wang and Wang* [1996].

[10] A variety of wavelet transforms are discussed in the literature, and are classified as either continuous or discrete [*Daubechies*, 1992]. We will show that both types of transforms are useful in the study of climatic time series, with the continuous wavelet transform (CWT) being the most suited to time series analysis as it contains information over a continuous domain of scales and times, and the discrete wavelet transform (DWT) being more suited for noise reduction and the compact representation of the time series. An extension of the DWT that has received less attention in the literature is as a preprocessing step to regression, and we will use this approach as an alternative to standard linear regression to evaluate the influence of ENSO on Australian rainfall time series.

2.2. Using Wavelets for Analysis

[11] If the time series can be represented as some continuous function $f(t)$, then the CWT can be represented as a function of two continuous variables by:

$$F(s,n) = |s|^{-1/2} \int f(t)\varphi_{s,n}(t)dt \qquad (1)$$

with

$$\varphi_{s,n}(t) = \varphi\left(\frac{t-n}{s}\right) \qquad (2)$$

where $\varphi_{s,n}$ are scaled and translated versions of the mother wavelet (φ), s is the wavelet scale and n is the localized time index, with both s and n defined as continuous real variables. The original signal can then be recovered through the inverse wavelet transform, which is defined as:

$$f(t) = \int\int F(s,n)\varphi_{s,n}dsdn \qquad (3)$$

In practice the time series is not represented as a continuous function but as a sequence of numbers denoted as x_t, so that the integrals can be evaluated as a summation over each data point in the signal. This is usually achieved as a convolution performed in Fourier space, with additional details provided in [*Torrence and Compo*, 1998]. The Morlet wavelet function was used for this study, since it has been shown to be well localized in both time and frequency [*Jevrejeva et al.*, 2003]. Note that since this wavelet is complex, the complex conjugate $\overline{\varphi}_{s,n}$ should be used instead of $\varphi_{s,n}$ in equation (1).

[12] The CWT allows for the construction of a wavelet spectrum which shows wavelet power (defined as $|F(s,n)|^2$) plotted against both time and frequency. This provides a large quantity of information about a time series, and for this reason can be difficult to interpret. To facilitate interpretation, the global wavelet spectrum may be used, and is defined as the time averaged power at a given frequency. Similarly, the scale average of the wavelet power is defined as the sum of the wavelet power spectrum between two scales, and can be useful to determine how wavelet power changes with time within a particular band [*Torrence and Compo*, 1998].

[13] Because of the non-Gaussian nature of many of the rainfall time series, a Monte Carlo approach was used to compute significance levels, which involved boot-strapping each rainfall time series to obtain new time series of the same duration (in this case 80 years) so that the underlying probability structure is preserved, and then conducting the wavelet analysis on each of the boot-strapped time series. This was repeated 10,000 times for each time series, so that consistent 95% confidence intervals could be obtained. No adjustment was made for red noise in the time series, as we found that statistically significant autocorrelation was not present at the 95% confidence level for the majority of time series analyzed.

2.3. Using Wavelets for Regression

[14] Like the CWT, the DWT provides a complete representation of the original time series using basis functions that are localized in both the time and the frequency domains. The difference is that for the DWT, the choice of scales s and translations n are restricted so that the wavelet function constitutes an orthonormal basis [*Daubechies*, 1992]. The advantage is that it provides a compact representation of the original time series, with the maximum number of wavelet basis functions equal to the number of data points in the original time series, N. This is

useful as a preprocessing step to regression, which is used here to isolate the influence of ENSO from the Australian rainfall time series as described in following sections. A flowchart of the general procedure followed is presented in Figure 2. Note that the logic in Figure 2 is meant to be inferred in conjunction with the description below.

[15] The relationship between the original time series and the scaled and translated wavelet function can now be written as:

$$x_t = \sum_{s,n} u_{s,n} \varphi_{s,n}(t) \tag{4}$$

where x_t represents the time series of length N, $u_{s,n}$ represents the set of wavelet coefficients, and $\varphi_{s,n}$ represents scaled and translated versions of the mother wavelet function as in equation (2), except that in this case we set:

$$s = 2^j \tag{5}$$

$$n = i2^j \tag{6}$$

where i and j are indices that can be any positive integer value defined over the time series. The Daubechies $d4$ transform is used as the wavelet function, since it is compactly supported and therefore lends itself well to the DWT, and comparison with several other wavelet functions showed that it provides an efficient representation of the original time series. The wavelet coefficients, $u_{s,n}$, can be calculated using the Mallat algorithm [*Alsberg et al.*, 1998], which involves applying a high-pass and a low-pass filter at each scale, s. The output from the high-pass filter at each scale is recorded as the wavelet coefficients. The low-pass filter extracts the low-frequency components for the next scale where another set of high- and low-pass filters are used. At each successive scale the number of wavelet basis functions (and hence the corresponding number of wavelet coefficients) is halved, in a process known as decimation [*Alsberg et al.*, 1998].

[16] Once the wavelet coefficients are obtained, it is possible to apply some form of noise reduction to the signal, with thresholding being one of the most popular methods currently available. The basis of this approach is that the low-energy wavelet coefficients represent white noise, while the underlying signal is represented by the high-energy coefficients. A number of thresholding methods are available, with universal thresholding being commonly used [*Johnstone and Silverman*, 1997]. This involves calculating a value of λ, and then setting to zero all wavelet coefficients that are lower than λ. A unique λ is calculated for each wavelet scale as follows:

$$\lambda_s = \sigma_s \sqrt{2 \log N} \tag{7}$$

where σ_s is a the standard deviation of the noise. This can be estimated as:

$$\sigma_s^2 = MAD\{u_{s,n}, n = 1, \ldots, 2^s\}/0.6745 \tag{8}$$

where MAD means the median absolute deviation and the constant 0.6745 is derived for Gaussian errors. This not only allows for the reduction in noise, but also ensures that the majority of the information of a time series is represented using only a limited number of wavelet coefficients.

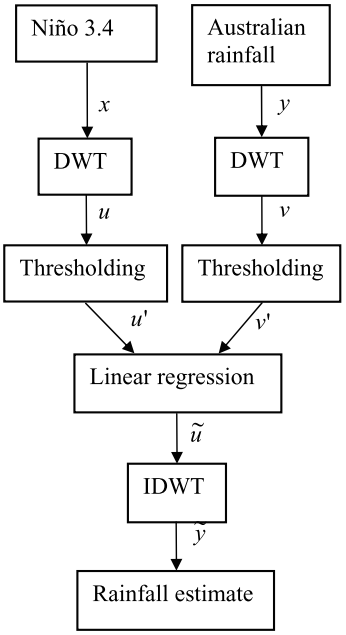

Figure 2. Approach used for wavelets regression, using a regression of an Australian rainfall time series against the Niño 3.4 time series as an example.

[17] Once the original time series has been transformed to the time-frequency domain and the noise has been reduced, it is now possible to commence wavelet regression, by applying standard linear regression techniques to the wavelet coefficients. Consider, for example, two time series denoted as x_t and y_t, with wavelet coefficients after thresholding given as $u'_{s,n}$ and $v'_{s,n}$. It is now possible to use standard linear regression methods, except that in this case the regression is performed over the frequency domain:

$$\hat{b}_s = \left(u_s'^T u_s'\right)^{-1} u_s'^T v_s' \tag{9}$$

where $\hat{b}_s$ represents an estimate of the least squares regression coefficient for the scale s. Note that the subscript n has been omitted as the regression is performed over the full coefficient vector for each scale. This provides a separate regression model at each scale, which may then be combined to form the full regression model. The limitation of this approach is that it does not consider variation in time, however this was considered necessary to avoid overparameterization of the regression model. For more sophisticated wavelet regression methods and extensions to multiple linear regression, refer to *Alsberg et al.* [1998].

[18] All that now remains is to calculate the new wavelet coefficients from the regression model, and to use an inverse DWT to convert the wavelet coefficients back to the time domain. This approach to wavelet regression is

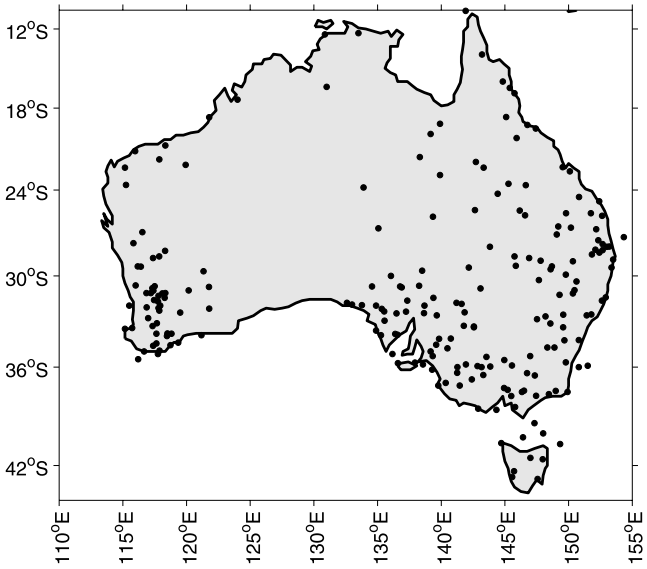

Figure 3. Location of rain gauge sites.

used to determine the contribution of ENSO on Australian rainfall time series, as summarized in Figure 2.

3. Data

3.1. Australian Rainfall

[19] The rainfall data used in this analysis are based on a set of high-quality rain gauges throughout Australia that were identified by *Lavery et al.* [1997]. For the purpose of this study, only those locations that contain records between 1922 and 2001 were used for this analysis. In regions where the records were sparse, some infilling of data was undertaken using nearby rain gauges, so that the final time series consisted of less than 1% missing data.

[20] In total, rainfall time series from 216 gauging stations were used, the locations of which are shown in Figure 3. These time series were broken down into (1) maximum annual daily rainfall, (2) the annual number of wet days (defined as >1 mm rainfall), and (3) the total annual rainfall, these variables being selected so as to provide inferences on the impact of climate variability on floods, droughts and the annual water budget. The analysis was conducted at the annual scale so as to focus on longer-term climatic variability and to remain consistent with the timescale used for the maximum annual daily rainfall time series, and any conclusions drawn from the analysis are limited to rainfall variability at this scale.

3.2. Climate

[21] The Niño 3.4 sea surface temperature (SST) data set was used as an indicator of the oceanic component of ENSO, and is defined as the seasonally averaged SST over the central-eastern equatorial Pacific (5°S–5°N, 120°W–170°W [*Trenberth*, 1997]). The extracted data set is from 1922 to 2001 to coincide with the duration of the rainfall data sets, and has been reconstructed using an optimal smoother of the raw sea surface temperature values as detailed by *Kaplan et al.* [1998]. These data were obtained from the International Research Institute for Climate Prediction (http://iri.columbia.edu). The annual average of this time series was used to facilitate comparison between the climatic data and the rainfall data series. Since the analysis considers rainfall variability over periods greater than 2 years, it is unlikely that the coarse resolution of this time series will significantly alter the wavelet results.

4. Results and Discussion

4.1. Relationship Between Australian Rainfall and ENSO

[22] Following the approach of a number of earlier studies [*Pittock*, 1975; *Nicholls and Woodcock*, 1981], we commenced the analysis by establishing the link between Australian rainfall and ENSO by examining the concurrent correlation between three series of Australian rainfall: the total annual rainfall, the maximum annual daily rainfall and the annual number of wet days, with the Niño 3.4 time series. The relationship between the Niño 3.4 time series and time series of Australian rainfall was considered to be statistically significant at the 95% confidence level for cases where the correlation coefficient was greater than 0.22. The results are presented in Figure 4, and show that statistically significant correlations are present between ENSO and both the total annual rainfall and the annual number of wet days in much of the eastern third of the continent. In contrast, the maximum annual daily rainfall did not exhibit any significant correlation with the Niño 3.4 time series for the majority of stations, with the stations that did exhibit significant correlations not showing any spatial trends. It is possible that the lower correlation coefficients for the latter time series are due to the more localized nature of large storm events, which are therefore more likely to appear as random time series when looking over the whole of Australia.

[23] The total annual rainfall results confirm the much more detailed correlation analysis presented by *Cai et al.* [2001] who found statistically significant correlation between Niño 3.4 and total annual rainfall for much of the eastern third of the continent over the period between 1889 and 1998. When *Cai et al.* [2001] broke these time series down into 10 year increments, however, the results showed that the regions of significant correlation were not consistent over time, but varied from year to year.

[24] These results highlight some of the limitations of correlation analysis, in that it is not able to easily capture the temporal and spatial variations of any linkages between ENSO and Australian rainfall. For example, the correlation results do not show how the strength of the relationship between ENSO and Australian rainfall is influenced by the IPO or Indian Ocean SSTs, as is suggested in the literature [e.g., *Nicholls*, 1989; *Drosdowsky*, 1993; *Power et al.*, 1999a]. In addition, it is known that correlation analysis is not very robust to outliers [*Wilks*, 1995], which means that it is difficult to establish whether statistically significant correlation reflects links between a large number of points over the time series, or whether it is simply an artifact of a relatively small number of extreme events.

[25] The wavelet analysis results presented in the subsequent sections aim to overcome these issues, by first examining how the dominant modes of variability change from one region to the next over the Australian continent using the global wavelet spectra for each time series, and

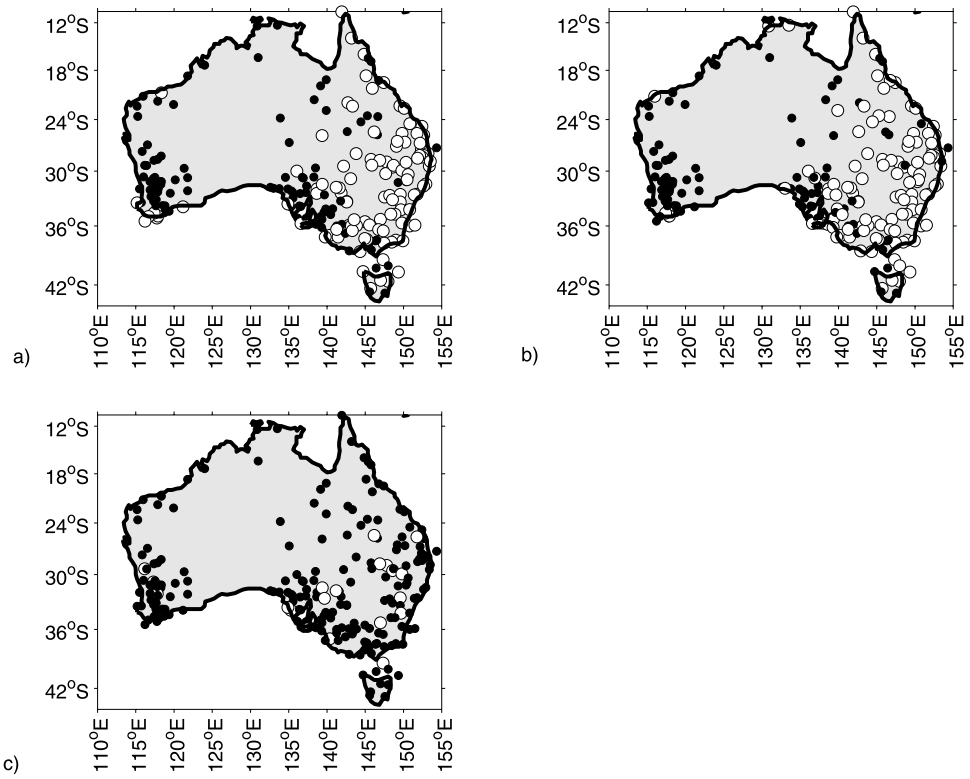

Figure 4. Concurrent correlation between the Niño 3.4 time series with (a) total annual rainfall, (b) annual number of wet days, and (c) maximum annual daily rainfall. Large open circles represent stations with correlations at or above the 95% significance level.

then by examining how these frequency modes change over time with the scale-averaged wavelet spectra.

4.2. Global Wavelet Spectrum of Australian Rainfall

[26] Having established the correlation between ENSO and several aspects of Australian rainfall time series, we will now examine whether a similar relationship can be found in the frequency domain using the global wavelet spectrum. The global wavelet spectrum for the Niño 3.4 time series was provided in Figure 1c, and shows that this time series has a spectral signature which is statistically significant with a period of 5 years. This is consistent with a range of previous studies, which generally place the ENSO spectra within bands such as the 3 to 6 year band [e.g., *Trenberth*, 1997] or the 2 to 8.5 year band [*Rodbell et al.*, 1999]. If the linkage between ENSO and Australian rainfall is as strong as is suggested by the correlation analysis, then similar spectra should be apparent for the total annual rainfall and the annual number of wet days over at least the eastern third of the continent.

[27] To verify whether this is the case, the global wavelet spectra were calculated for the total annual rainfall, the annual number of wet days and the maximum annual daily rainfall, for periods ranging between 2 years and 32 years. Of these periods, distinct regions of statistically significant variability were found at periods of 2.6, 4.6, 7 and 13 years for both the total annual rainfall and the annual number of wet days, with the remaining periods providing only limited additional information. A Fourier analysis was performed to verify the validity of the wavelets results, and the two methods were found to be in agreement for the vast majority of rainfall gauging stations.

[28] For each of these periods, an examination of the regions of statistical significance for the total annual rainfall time series is presented in Figure 5. On the basis of these results it is immediately apparent that, of the region on the eastern third of the continent in which there is significant correlation with the Niño 3.4 time series, there are only two areas – one in the southern part of the continent with a period of 4.6 years and the other in the east with a period of 7 years – that operate at a periodicity that is similar to the Niño 3.4 time series. In contrast, there is also an area along the east coast of Australia with a period of 13 years that exhibits a distinctly different spectral signature to that of the Niño 3.4 time series. Although the figures are not shown here, it is interesting to note that very similar results were obtained for the annual number of wet days, which is also correlated with the Niño 3.4 time series. Readers should note that significance is assessed on the basis of the results for individual point locations, and not on a regional basis. While results at individual stations may be affected by the proportion of the noise that is present in each time series, identification of distinct regions where similar patterns are observed imparts greater confidence in the results than is represented by the confidence intervals indicated.

[29] In the analysis of maximum annual daily rainfall, it was found that although some individual time series were significant at various periods within the 2 to 32 year band, it was not possible to identify any regions of coherent variability. Furthermore, the number of such time series gener-

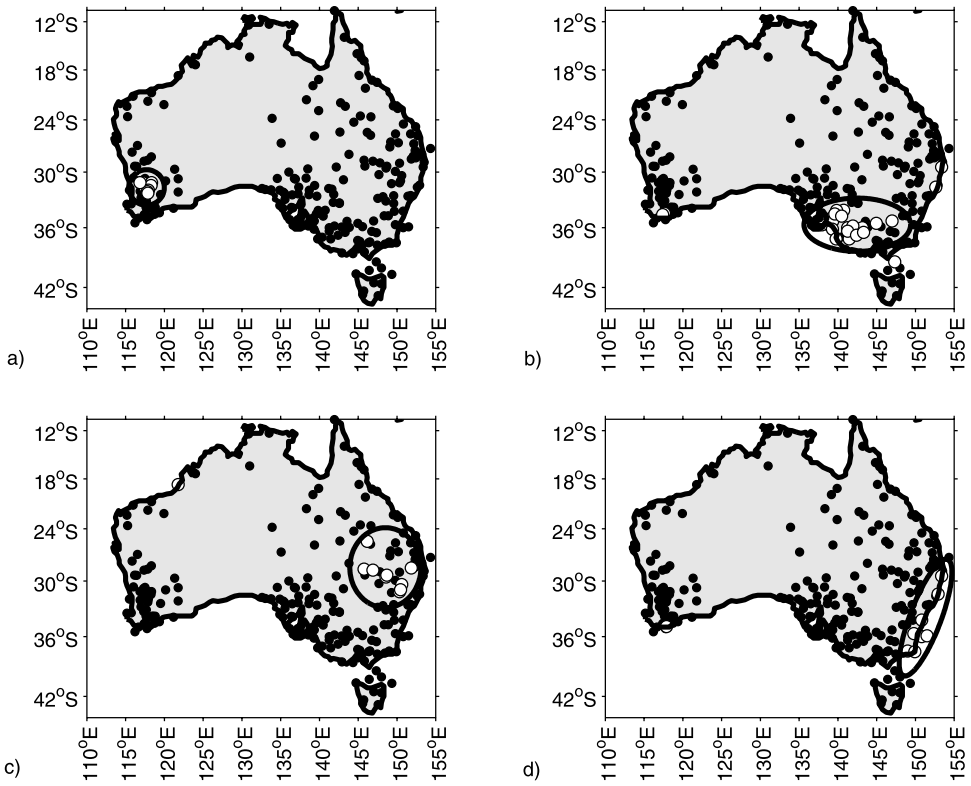

Figure 5. Regions of significant variability for series of total annual rainfall with periods of (a) 2.6 years, (b) 4.6 years, (c) 7 years, and (d) 13 years. Large open circles represent stations with correlations at or above the 95% significance level.

ally did not exceed 5% of the total number of time series analyzed, thereby reflecting the number of statistically significant time series expected by random chance when using 95% significance levels. Therefore, as the maximum annual daily rainfall is the time series that is commonly used for flood frequency analysis, these results suggest that the larger storm events are not influenced by long-term climatic phenomena to the same extent as the long-term averages. It is interesting to note that a range of studies [*Jain and Lall*, 2001; *Kiem et al.*, 2003; *Verdon et al.*, 2004] have discussed evidence of long-term climate variability in maximum annual daily streamflow time series, suggesting that streamflow variability is largely due factors such as moisture conditions in the catchment rather than the more intense bursts of rainfall captured in the maximum annual daily rainfall time series. This is in agreement with the studies of *Chen and Kumar* [2002] who suggest that the storage effects of soil moisture can have a significant influence on the low-frequency variability of streamflow in North America.

4.3. Rainfall Variability Over Time

[30] It is clear from the preceding analysis that the regions of coherent variability using the global wavelet spectra do not coincide with the region of significant correlation on the eastern third of the continent, suggesting that the wavelet analysis and the correlation analysis highlight different aspects of climate variability in Australia. We now examine whether similar results can be found in the time domain, by examining the wavelet spectra of several representative time series in more detail. These representative time series were constructed for each of the regions circled in Figure 5, and were calculated using the mean of all the time series which exhibited variability at or above the 95% confidence level. The focus on mean rainfall across a number of gauging stations within a given region was necessary to simplify the presentation, and ensured that the analysis focused on those aspects that are common to all the time series within that region. Only the total annual rainfall time series is presented here, with similar results obtained for the annual number of wet days. The maximum annual daily rainfall time series were not considered, as regions of coherent variability could not be identified in either the correlation or the global wavelet analyses.

[31] The scale-averaged wavelet spectra were calculated for the 3 to 6 year band for each region. While we acknowledge that this band is relatively narrow and that the ENSO phenomenon may operate at a wider range of periodicities such as in the 2 to 8.5 year band [*Rodbell et al.*, 1999], we selected a narrow band as we consider this band to be most strongly influenced by ENSO, so that the results are least likely to be distorted by variability that is not due to ENSO. We have also calculated the results for some of these wider bands (such as the 2 to 8.5 year band), and we have found these results to be consistent with the results in the 3 to 6 year band presented here. These results are presented in Figure 6, and may be compared with the scale-averaged Niño 3.4 spectrum that was presented in Figure 1e. An examination of the peaks and troughs of each time series reveals that important differences can be observed between each region of coherent variability, as well as between the

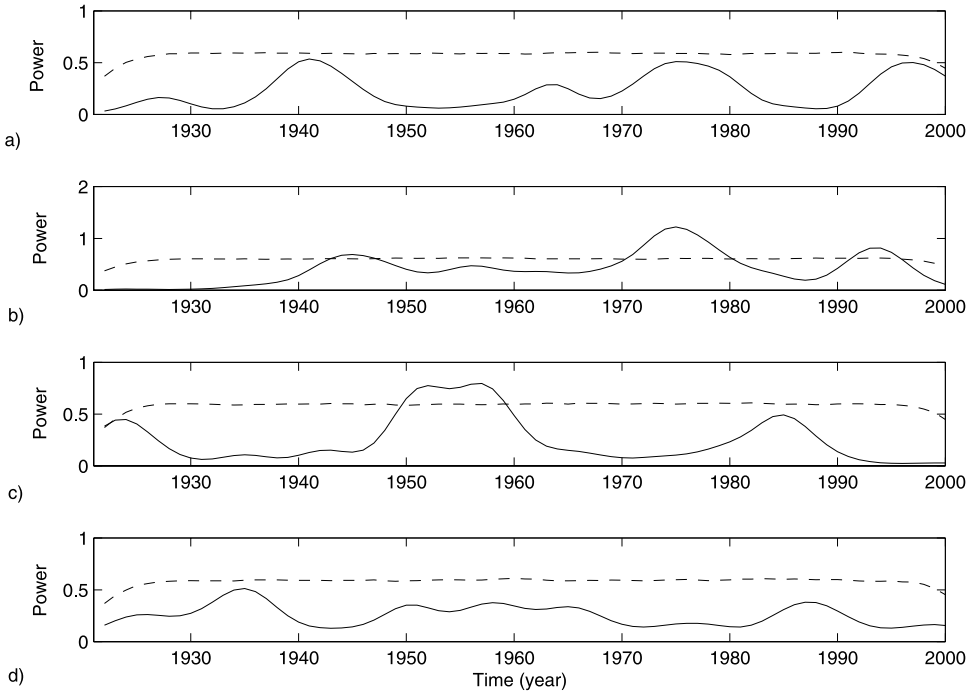

Figure 6. Scale-averaged wavelet power spectra for the 3 to 6 year band, corresponding to the regions identified in Figures 5a, 5b, 5c and 5d, respectively. Dashed line represents the confidence limits at the 95% significance level.

rainfall time series and Niño 3.4. It is therefore apparent that the times when the ENSO phenomenon exhibits the highest variability in the 3 to 6 year frequency range do not coincide with the times when the Australian rainfall exhibits the highest variability.

4.4. Regions of Coherent Variability After Excluding the Influence of ENSO

[32] On the basis of the wavelets results presented above, it is apparent that the regions of coherent variability exhibit both a significantly different spatial pattern to the region of statistically significant correlation with the Niño 3.4 index as depicted in Figure 4, and a different temporal structure to the Niño 3.4 index in the 3 to 6 year band. It still is not evident, however, whether these results are due to complex nonlinear interactions between ENSO and Australian rainfall at a range of different frequencies, or whether the coherent climate variability derived from the wavelet analysis is not related to ENSO at all.

[33] One method to determine which of these hypotheses are correct is to extract the influence of ENSO from the Australian rainfall time series through some regression model, and then perform the wavelet analysis on the residual time series. If the regions of coherent variability are still present, then it is unlikely that these regions could be attributable to ENSO, while the removal of variability would suggest that the wavelet spectra are somehow linked to ENSO.

[34] The wavelet regression methodology that was outlined in section 2.3 was used for the analysis, and contains some important advantages over standard linear regression, including the ability of the method (1) to account for any noise in the signal, (2) to account for some of the nonstationarity that is present in the relationship between ENSO and Australian rainfall, and (3) to ensure that the regression parameters are less sensitive to any extreme values in the original data.

[35] After the regression in the wavelet domain, a continuous wavelet transform was applied to the residuals, and the global wavelet spectra were calculated using the same approach that was used in section 4.2. The results for the residuals from the total annual rainfall time series at periods of 2.6, 4.6, 7 and 13 years are shown in Figure 7, these periods being selected so that they can be compared directly to the global wavelet spectra of the original time series. A comparison of Figures 5 and 7 shows that, for the overwhelming majority of rainfall time series, the wavelet regression did not have a significant impact on the variability at each period, suggesting that the variability was not directly linked to the ENSO phenomenon. While this could be expected for the regions with periods not directly associated with the ENSO (such as region along the east coast with a period of 13 years), the results for the ENSO related periodicities are further indication of the low correspondence the ENSO signal has with the 3 to 6 year variability observed in Australian rainfall. A similar analysis was also conducted using standard linear regression, and the results from this alternative method yielded very similar results to the wavelets regression approach.

[36] The close agreement between two conceptually different methods of extracting the influence of ENSO from the rainfall time series adds further weight to the hypothesis that the periodicities in each of the regions distinct from ENSO, suggesting that any method to forecast rainfall in

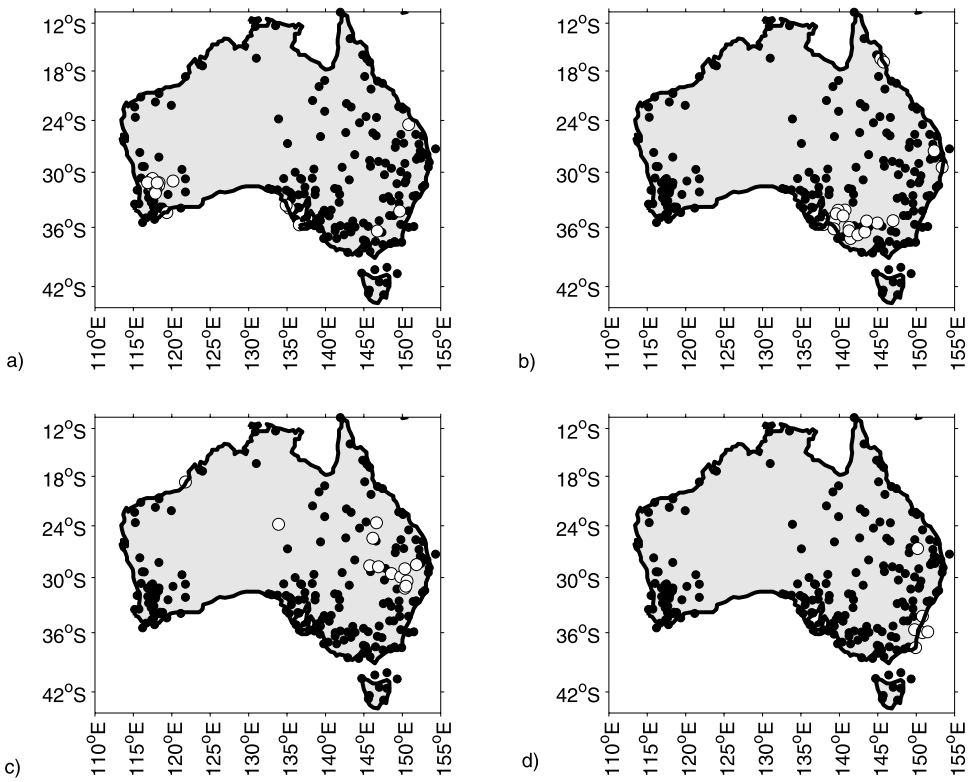

Figure 7. Regions of significant variability after the effects of ENSO have been removed, with periods of (a) 2.6 years, (b) 4.6 years, (c) 7 years, and (d) 13 years. Large open circles represent stations with correlations at or above the 95% significance level.

Australia at the annual scale should look beyond ENSO if it to be successful in accounting for all the major sources of variability in Australian rainfall.

5. Conclusions

[37] One of the key aspects to better managing water resources in Australia is to understand the causes of medium- to long-term rainfall variability, which is known to result in both droughts and periods of above average rainfall and flooding. This variability is frequently regarded as being caused by climatic phenomena such as ENSO, which has been shown previously to exert a highly nonstationary influence on Australian rainfall [e.g., *McBride and Nicholls*, 1983; *Power et al.*, 1998]. In this study, we used the method of wavelets to analyze time series of maximum annual daily rainfall, the annual number of wet days, and the total annual rainfall, with the aim of examining whether wavelets could assist in identifying dominant modes of rainfall variability, and determining the extent to which this variability could be explained by the ENSO phenomenon.

[38] In the case of the maximum annual daily rainfall time series, it was not possible to identify any regions of coherent variability using the wavelet analysis, thus confirming the results of the correlation analysis which was unable to find a statistically significant relationship between this time series and ENSO. This has important implications for flood frequency analysis, since the long-term variability that is known to occur in streamflow is not adequately represented in the maximum annual daily rainfall time series, and may therefore be attributable to other factors such as antecedent moisture content.

[39] In contrast, using the wavelet analysis on the total annual rainfall and the annual number of wet days showed four regions of coherent variability over the Australian continent, which are summarized as follows: (1) a region in the southwest of Australia with a dominant mode of variability with a period of 2.6 years, (2) a region in the south of Australia with a dominant mode of variability with a period of 4.6 years, (3) a region in central and eastern Australia with a dominant mode of variability with a period of 7 years, and (4) a region along the east coast of Australia with a dominant mode of variability with a period of 13 years.

[40] When comparing this to the results from the correlation analysis with ENSO, it was observed that, while the variability at the 4.6 year period in the south of Australia and possibly the variability with a period of 7 years in eastern Australia operated at a similar frequency to ENSO, the remaining rainfall time series contained variability which was outside the ENSO band. An analysis of the scale-averaged wavelet spectra from the regionally averaged time series was also unable to establish a link between ENSO and the rainfall variability in each of these regions, by showing that the times of maximum variability in the 3 to 6 year band for the Niño 3.4 time series did not correspond to the times of maximum variability in the same frequency for Australian rainfall.

[41] To test whether the discrepancy between the correlation and the wavelet results was due to the nonstationary

nature of the ENSO phenomenon on Australian rainfall or due to some as yet unknown influence, a wavelet regression was performed to extract the ENSO signal from the Australian rainfall time series. The residuals from the regression were then reanalyzed, and it was shown that the regions of coherent variability remained unchanged and therefore are not attributable to ENSO.

[42] The results of this study clearly show that, not only is the ENSO phenomenon not captured by the spectral analysis for each of the time series examined here, but that there are regions of significant variability that are not accounted for by ENSO. It is therefore necessary to look beyond ENSO if we are to obtain a more complete picture of what causes the medium- to long-term variability in Australian rainfall at the annual scale.

[43] **Acknowledgments.** This research was funded by the Australian Research Council and Sydney Catchment Authority. Comments from the anonymous JGR reviewers are gratefully acknowledged.

References

Alsberg, B. K., A. M. Woodward, M. K. Winson, J. J. Rowland, and D. B. Kell (1998), Variable selection in wavelet regression models, *Anal. Chim. Acta*, *368*(1–2), 29–44.

Cai, W., P. H. Whetton, and A. B. Pittock (2001), Fluctuations of the relationship between ENSO and northeast Australian rainfall, *Clim. Dyn.*, *17*(5–6), 421–432.

Chen, J., and P. Kumar (2002), Role of terrestrial hydrologic memory in modulating ENSO impacts in North America, *J. Clim.*, *15*(24), 3569–3585.

Chiew, F. H. S., T. C. Piechota, J. A. Dracup, and T. A. McMahon (1998), El Nino/Southern Oscillation and Australian rainfall, streamflow and drought: Links and potential for forecasting, *J. Hydrol.*, *204*, 138–149.

Cordery, I., and Y. Opoku-Ankomah (1994), Temporal variation of relations between tropical sea-surface temperatures and New South Wales Rainfall, *Aust. Meteorol. Mag.*, *43*(2), 73–80.

Daubechies, I. (1992), *Ten Lectures on Wavelets*, Soc. for Ind. and Appl. Math., Philadelphia, Pa.

Drosdowsky, W. (1993), Potential predictability of winter rainfall over southern and eastern Australia using Indian Ocean sea-surface temperature anomalies, *Aust. Meteorol. Mag.*, *42*, 1–6.

Drosdowsky, W. (2002), SST phases and Australian rainfall, *Aust. Meteorol. Mag.*, *51*, 1–12.

Gu, D., and S. G. H. Philander (1995), Secular changes of annual and interannual variability in the tropics during the past century, *J. Clim.*, *8*, 864–876.

Jain, S., and U. Lall (2001), Floods in a changing climate: Does the past represent the future?, *Water Resour. Res.*, *37*, 3193–3205.

Jevrejeva, S., J. C. Moore, and A. Grinsted (2003), Influence of the Arctic Oscillation and El Nino-Southern Oscillation (ENSO) on ice conditions in the Baltic Sea: The wavelet approach, *J. Geophys. Res.*, *108*(D21), 4677, doi:10.1029/2003JD003417.

Johnstone, I. M., and B. W. Silverman (1997), Wavelet threshold estimators for data with correlated noise, *J. R. Stat. Soc., Ser. B Methodol.*, *59*(2), 319–351.

Kaplan, A., M. A. Cane, Y. Kushnir, A. C. Clement, M. B. Blumenthal, and B. Rajagopalan (1998), Analyses of global sea surface temperature 1856–1991, *J. Geophys. Res.*, *103*(C9), 18,567–18,589.

Kiem, A. S., S. W. Franks, and G. Kuczera (2003), Multi-decadal variability of flood risk, *Geophys. Res. Lett.*, *30*(2), 1035, doi:10.1029/2002GL015992.

Lau, K. M., and H. Y. Weng (1995), Climate signal detection using wavelet transform: How to make a time series sing, *Bull. Am. Meteorol. Soc.*, *76*, 2391–2402.

Lavery, B., G. Joung, and N. Nicholls (1997), An extended high-quality historical rainfall dataset for Australia, *Aust. Meteorol. Mag.*, *46*, 27–38.

Mantua, N. J., S. R. Hare, Y. Zhang, J. M. Wallace, and R. C. Francis (1997), A Pacific interdecadal climate oscillation with impacts on salmon production, *Bull. Am. Meteorol. Soc.*, *78*(6), 1069–1079.

McBride, J. L., and N. Nicholls (1983), Seasonal relationships between Australian rainfall and the Southern Oscillation, *Mon. Weather Rev.*, *11*, 1998–2004.

Nicholls, N. (1989), Sea surface temperatures and Australian winter rainfall, *J. Clim.*, *2*, 965–973.

Nicholls, N., and F. Woodcock (1981), Verification of an empirical long-range weather forecasting technique, *Q. J. R. Meteorol. Soc.*, *107*(454), 973–976.

Nicholls, N., B. Lavery, C. Frederiksen, W. Drosdowsky, and S. Torok (1996), Recent apparent changes in relationships between the El Niño–Southern oscillation and Australian rainfall and temperature, *Geophys. Res. Lett.*, *23*(23), 3357–3360.

Pittock, A. B. (1975), Climatic change and patterns of variation in Australian rainfall, *Search*, *6*(11-1), 498–504.

Power, S., E. Tseitkin, S. Torok, B. Lavey, R. Dalini, and B. McAvaney (1998), Australian temperature, Australian rainfall and the Southern Oscillation, 1910–1992: Coherent variability and recent change, *Aust. Meteorol. Mag.*, *47*, 85–101.

Power, S., T. Casey, C. Folland, A. Colman, and V. Mehta (1999a), Inter-decadal modulation of the impact of ENSO on Australia, *Clim. Dyn.*, *15*(5), 319–324.

Power, S., F. Tseitkin, V. Mehta, B. Lavery, S. Torok, and N. Holbrook (1999b), Decadal climate variability in Australia during the twentieth century, *Int. J. Climatol.*, *19*(2), 169–184.

Quayle, E. T. (1929), Long range rainfall forecasting from tropical (Darwin) air pressures, *Proc. R. Soc. Victoria*, *41*, 160–164.

Rodbell, D. T., G. O. Seltzer, D. M. Anderson, M. B. Abbott, D. B. Enfield, and J. H. Newman (1999), An approximately 15,000-year record of El Niño-driven alluviation in southwestern Ecuador, *Science*, *283*, 516–520.

Torrence, C., and G. P. Compo (1998), A practical guide to wavelet analysis, *Bull. Am. Meteorol. Soc.*, *79*(1), 61–78.

Torrence, C., and P. J. Webster (1998), The annual cycle of persistence in the El Niño Southern Oscillation, *Q. J. R. Meteorol. Soc.*, *124*(550), 1985–2004.

Trenberth, K. E. (1997), The definition of El Niño, *Bull. Am. Meteorol. Soc.*, *78*, 2771–2777.

Verdon, D. C., A. M. Wyatt, A. S. Kiem, and S. W. Franks (2004), Multi-decadal variability of rainfall and streamflow: Eastern Australia, *Water Resour. Res.*, *40*, W10201, doi:10.1029/2004WR003234.

Wang, B., and Y. Wang (1996), Temporal structure of the Southern Oscillation as revealed by waveform and wavelet analysis, *J. Clim.*, *9*, 1586–1598.

Wilks, D. S. (1995), *Statistical Methods in the Atmospheric Sciences*, Elsevier, New York.

Zhang, Y., J. M. Wallace, and D. S. Battisti (1997), ENSO-like interdecadal variability: 1900–93, *J. Clim.*, *10*(5), 1004–1020.

A. Sharma and S. Westra, School of Civil and Environmental Engineering, University of New South Wales, Sydney, NSW 2052, Australia. (seth@civeng.unsw.edu.au; a.sharma@unsw.edu.au)